

Au₁₃₃(SPh-*t*Bu)₅₂ Nanomolecules: X-ray Crystallography, Optical, Electrochemical, and Theoretical Analysis

Amala Dass,^{*,†} Shevanuja Theivendran,^{†,#} Praneeth Reddy Nimmala,^{†,#} Chanaka Kumara,[†] Vijay Reddy Jupally,^{†,⊥} Alessandro Fortunelli,[‡] Luca Sementa,^{‡,#} Giovanni Barcaro,^{‡,#} Xiaobing Zuo,[§] and Bruce C. Noll^{||}

[†]Department of Chemistry and Biochemistry, University of Mississippi, Oxford, Mississippi 38677, United States

[‡]CNR-ICCOM & IPCF, Consiglio Nazionale delle Ricerche, Pisa, I-56124, Italy

[§]X-ray Science Division, Advanced Photon Source, Argonne National Laboratory, Argonne, Illinois 60439, United States

^{||}Bruker AXS Inc., 5465 East Cheryl Parkway, Madison, Wisconsin 53711, United States

S Supporting Information

ABSTRACT: Crystal structure determination has revolutionized modern science in biology, chemistry, and physics. However, the difficulty in obtaining periodic crystal lattices which are needed for X-ray crystal analysis has hindered the determination of atomic structure in nanomaterials, known as the “nanostructure problem”. Here, by using rigid and bulky ligands, we have overcome this limitation and successfully solved the X-ray crystallographic structure of the largest reported thiolated gold nanomolecule, Au₁₃₃S₅₂. The total composition, Au₁₃₃(SPh-*t*Bu)₅₂, was verified using high resolution electrospray ionization mass spectrometry (ESI-MS). The experimental and simulated optical spectra show an emergent surface plasmon resonance that is more pronounced than in the slightly larger Au₁₄₄(SCH₂CH₂Ph)₆₀. Theoretical analysis indicates that the presence of rigid and bulky ligands is the key to the successful crystal formation.

Gold nanomolecules or nanocrystal molecules¹ are ultra-small, typically <3 nm, thiolated gold nanoparticles with a precise number of metal Au atoms and protecting organic thiolate ligands. These compounds possess unique electrochemical² and optical properties³ which make them promising in a variety of applications, ranging from catalysis to biomedicine.⁴ However, a deeper understanding of structure–property relationships for these materials is hindered by the difficulties in determining their crystal structure due to the nanostructure problem,⁵ especially for the larger compounds which are the most appealing for many applications. While some crystal structures have been reported,^{6–8} these are mostly of smaller sizes, with the largest compound being Au₁₀₂(SC₆H₄–COOH)₄₄. The X-ray crystal structure of the larger, stable, and robust Au₁₄₄(SCH₂CH₂Ph)₆₀ nanomolecule is still an *unresolved* mystery, although it has been sought after for more than a decade.

Herein we report the following: (a) the crystal structure of an unprecedentedly large Au thiolate Au₁₃₃S₅₂ nanomolecule, using a rigid and bulky aromatic ligand, with a precise number of Au metal atoms and organic ligands and exhibiting a peculiar

hybrid structure reported here for the first time; (b) isolating this molecular substance in large quantity and verifying its composition using ESI and MALDI MS; (c) characterizing its optical and electrochemical properties; and (d) developing a theoretical analysis of the full Au₁₃₃(SPh-*t*Bu)₅₂ nanomolecule elucidating its electronic structure as well as geometrical and optical properties, thus achieving a consistent picture of its structure and properties through an excellent agreement of theoretical and experimental data and clarifying the reasons for its successful crystal formation.

The structure of the Au₁₃₃(SPh-*t*Bu)₅₂ nanomolecule was solved in the C2/*c* space group to an *R*₁ value of 8.41% (Table S1). Figure 1 shows the atomic structure of the metal–sulfur core, Au₁₃₃S₅₂. The structure consists of a central Au atom, surrounded by 12 Au atoms along the vertices of an icosahedron, Figure 1a. This Au₁₂ shell is covered by a second Au₄₂ shell also in an icosahedral configuration, Figure 1b, further enclosed by a Au₅₂ shell, which is derived from the 60-atom rhombicosidodecahedron⁹ lacking 8 atoms, Figure 1c. The final layer is composed of Au₂₆(SR)₅₂, or 26 units of [–SR–Au–SR–] staples, Figure 1d,e. The coordinates of the –Ph-*t*Bu ligands were not fully determined by X-ray data (see Supporting Information for details), due to the difficulty in accounting for organic ligands in large clusters as reported before, e.g., for Pd systems,¹⁰ but the total composition including the ligands was confirmed using mass spectrometry and theoretical calculations, *vide infra*. The Au₅₅ core (1 + 12 + 42 atoms) with a complete 60-atom rhombicosidodecahedral shell was first observed in Pd₁₄₅ and Pd₁₆₅ structures reported by Dahl’s group^{9,10} and are the basis for the proposed Au₁₄₄ structural model.¹¹

However, the geometry of the present Au₁₀₇ core structure is peculiarly transformed from a rhombicosidodecahedron into a hybrid structure which to the best of our knowledge is reported here for the first time. This is obtained by first merging 4 Au triangles from the Au₆₀ shell (whose centers lie at the vertex of a tetrahedron) into single Au atoms (see Figure 1f). This reduces the steric hindrance of the bulky SPh-*t*Bu ligands but lowers the point group symmetry from *I*_h to *T*. A minor

Received: December 26, 2014

Published: April 2, 2015

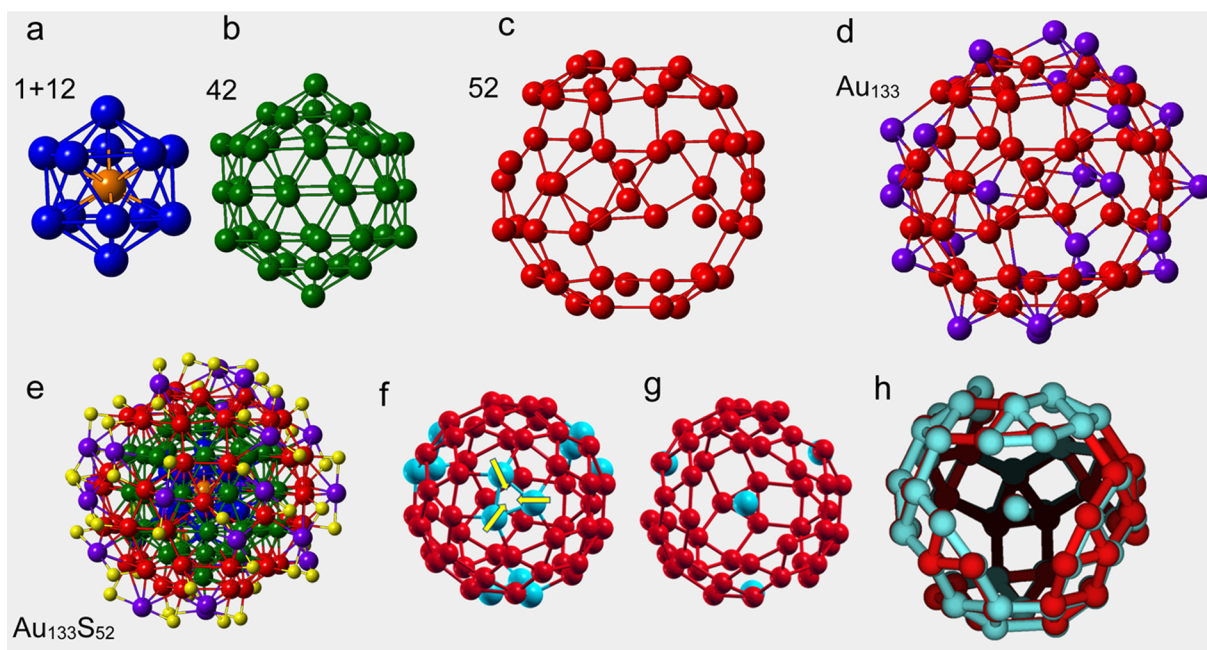


Figure 1. X-ray crystallographic structure of the $\text{Au}_{133}\text{S}_{52}$ core of $\text{Au}_{133}(\text{SPh-}t\text{Bu})_{52}$ nanomolecules. (a) Au_{12} icosahedral shell surrounding the central Au atom; (b) Au_{42} icosahedral shell; (c) 52-atom shell whose structure is derived from a 60-atom rhombicosidodecahedron with 8 atoms missing; (d) Au_{133} core geometry showing the outmost 26 atoms that are part of the 26 $[-\text{SR}-\text{Au}-\text{SR}-]$ units; (e) $\text{Au}_{133}\text{S}_{52}$ structure; (f) merging of four Au_3 triangles (colored in light blue) in the 60-atom rhombicosahedral shell into a single Au atom; (g) 52-atom shell resulting from step (f); (h) minor rearrangement of the 52-atom shell to produce the final structure, coinciding with that of (c), with initial positions in red and final positions in light blue.

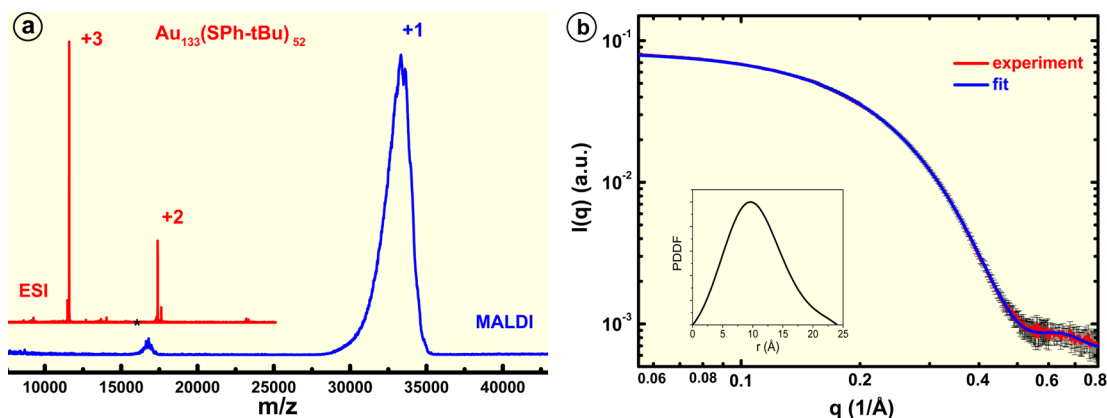


Figure 2. (a) Mass spectrometry. MALDI (blue) and ESI (red) mass spectra of $\text{Au}_{133}(\text{SPh-}t\text{Bu})_{52}$ nanomolecules. (b) X-ray scattering data (red curve with black error bars), GNOM fitting¹³ (blue) and pair distance distribution function (PDDF, inset).

rearrangement of the Au_{52} shell further lowers the symmetry to a chiral D_2 structure (see Figure 1g–h). Especially the central Au atom is unexpected given the widely accepted Au_{144} theoretical model which contains a Au_{12} core with no central atom.¹²

Geometry of the Au_{133} nanomolecule is thus organized in shells: the first shell is occupied by a central Au atom and the second shell corresponds to an icosahedron of 12 vertices; the third shell contains 42 atoms which are positioned both on-top of the 12 corners and at the middle of the 30 edges of the inner 12-atom icosahedron; the structure obtained is the well-known Mackay icosahedron of 55 atoms. A further growth of 60 atoms will lead to the formation of the 115-atom dodecahedron with full I_h symmetry observed in the Pd_{145} structure;¹⁰ this growth mode corresponds to the occupation of the anti-Mackay sites by the outer gold atoms, which would occupy all the 60 hollow

sites of the inner 55-atom icosahedron. However, in the 133-Au atom structure only 52 atoms are found in the fourth shell, with a peculiar reconstruction described above. A final fifth shell of 26 atoms—instead of 30, as in the case of the Pd_{145} compound—completes the structure of the gold core with a complete loss of symmetry. The greater sparsity in the last two shells corresponds to a slight contraction of the shell radii; by comparing the present structure with the powder XRD from ref 12, we observe the following values: in the fourth shell of 52 atoms of the 133-Au atom structure, an average radius of 6.87 Å with respect to a radius of 7.10 Å for the 60-atom shell of the theoretically predicted Au_{144} model; in the fifth shell of 26 atoms of the 133-Au atom structure, an average radius of 8.47 Å with respect to a radius of 9.03 Å for the 30-atom shell of the 144-Au atom model.

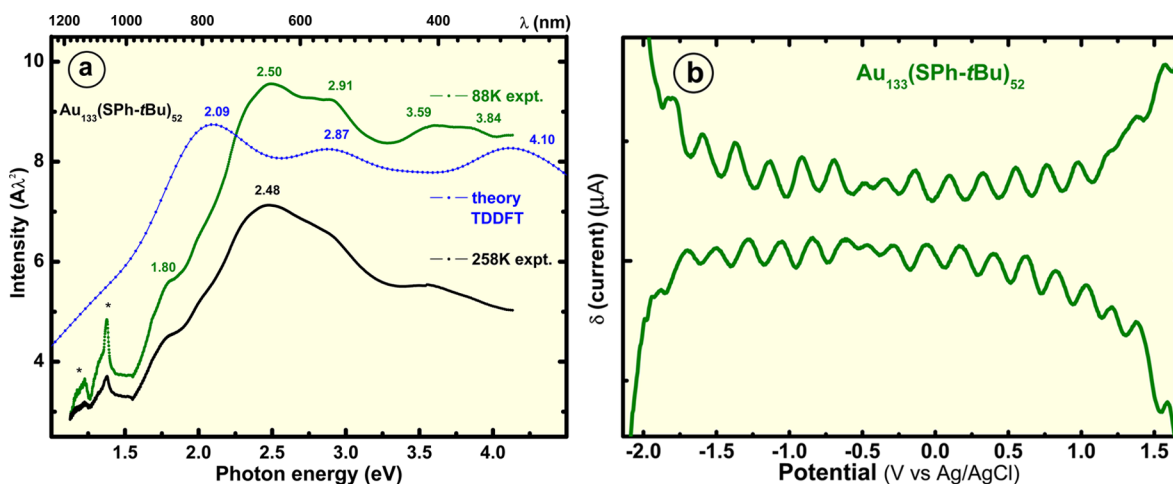


Figure 3. (a) UV-vis spectrum of $\text{Au}_{133}(\text{SPh-}t\text{Bu})_{52}$ nanomolecules in 3-MeTHF at 258 K (black) and 88 K (green). Theoretically predicted TDDFT spectrum is shown in blue. (b) Electrochemical differential pulse voltammetry (DPV) of $\text{Au}_{133}(\text{SPh-}t\text{Bu})_{52}$. Asterisks in (a) indicates peaks due to instrumental artifacts.

$\text{Au}_{133}(\text{SPh-}t\text{Bu})_{52}$ was synthesized and purified using size exclusion chromatography in large quantities, and its composition and purity were verified using mass spectrometry.¹³ In Figure 2a, the blue curve shows the MALDI-MS using DCTB matrix,¹⁴ with one broad dominant feature centered $\sim 33\,000$ m/z and a minor feature centered $\sim 16\,000$ m/z , corresponding to the singly and doubly charged molecular ions, respectively. ESI-MS, shown in the red spectrum in Figure 2a, contains two peaks at 11 596.7 and 17 395.8 m/z corresponding to the 3+ and 2+ ions of $\text{Au}_{133}(\text{SPh-}t\text{Bu})_{52}$, respectively. The theoretical values for the 3+ and 2+ ions are 11 596.8 and 17 395.2 m/z , with a mass error of 8 and 34 ppm, respectively. Intentional addition of cesium acetate¹³ resulted in $[\text{Au}_{133}(\text{SPh-}t\text{Bu})_{52}\cdot 2\text{Cs}^+]^{3+}$ as a major adduct, indicating that the +1 is the preferred charge state in agreement with theoretical analysis, *vide infra*. MALDI-MS data (Figure 2a), including the expanded mass range (Figure S3), and at very high laser fluence (Figure S4, S5) show that the final product is highly pure, without any other core sizes. Unfragmented and high resolution ESI MS yields the $\text{Au}_{133}(\text{SPh-}t\text{Bu})_{52}$ composition, confirming the crystallographic results. Additional supporting evidence for the nanoparticle size, and purity were provided by small-angle X-ray scattering (SAXS) and transmission electron microscopy (TEM) (Figure S1). SAXS data fitting up to 0.8 Å shows that the diameter is in agreement with MS and X-ray results (Figure 2b), and the uniform size was demonstrated by the wide range of linear Guinier behavior ($\ln[I(q)]$ vs q^2 (Figure S6).

The optical spectra at two different temperatures, shown in Figure 3a, display distinct features³ at 2.49 eV and between 3.59 and 3.81 eV, with a secondary peak at 2.91 eV. The peaks at 2.49 and 2.91 eV are reminiscent of the surface plasmon resonance and are more pronounced than in $\text{Au}_{144}(\text{SCH}_2\text{CH}_2\text{Ph})_{60}$.¹⁵ Differential pulse voltammogram, Figure 3b, shows 17 distinct redox waves, a number larger than the 15 waves¹⁶ reported for $\text{Au}_{144}(\text{SCH}_2\text{CH}_2\text{Ph})_{60}$, whose positions are different than those of Au_{130} or Au_{144} .²

Theoretical analysis fully supports the experimental assignment and provides a framework for the interpretation of experimental results. Starting from the experimental X-ray geometry of the $\text{Au}_{133}\text{S}_{52}$ core, all incomplete ligands were removed, and 52 $-\text{Ph-}t\text{Bu}$ groups were added and this initial

structure was subjected to local relaxation followed by two 1 ps runs of ab initio Molecular Dynamics (AIMD) based on a density-functional theory (DFT) approach: a first AIMD run at 900 K to allow the initial guess to exit possible metastable local minima, and a second AIMD run at 300 K to produce equilibrated coordinates.¹³ The geometry of $\text{Au}_{133}(\text{SPh-}t\text{Bu})_{52}$ obtained by a final local relaxation is shown in Figure 4 and is reported in the Supporting Information.¹³

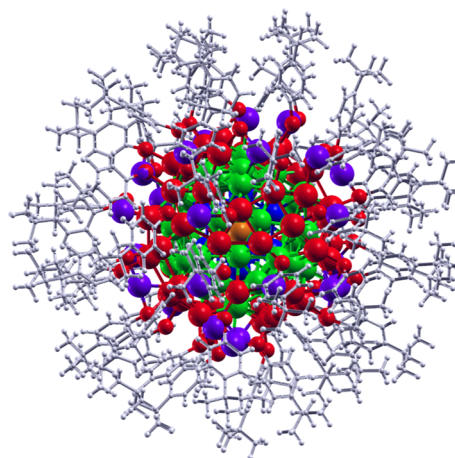


Figure 4. Theoretically predicted geometry of the $\text{Au}_{133}(\text{SPh-}t\text{Bu})_{52}$ nanomolecule. See text for more details. Color coding the same as that in Figure 1, and C and H atoms are displayed in light gray.

The $-\text{SPh-}t\text{Bu}$ ligands play a crucial role in determining the structure. Replacement of nonbulky ligands as in $\text{Au}_{144}(\text{SCH}_2\text{CH}_2\text{Ph})_{60}$ with bulkier phenyl groups in fact creates a steric repulsion in proximity of the Au cluster which is alleviated by decreasing the thiolate surface density,¹⁷ with the average surface area per sulfur atom increasing from 18.8 to 19.2 Å² in passing from $\text{Au}_{144}\text{S}_{60}$ to $\text{Au}_{133}\text{S}_{52}$. We estimate the residual steric repulsion in $\text{Au}_{133}(\text{SPh-}t\text{Bu})_{52}$ to be ~ 1.6 eV via an energy decomposition analysis^{13,18} thus being minor in such a large compound. At this decreased thiolate surface density, the rigid p - $t\text{Bu}$ groups play an important role, as they provide an outer protective layer which has the double effect of (i) reducing the cluster structural freedom and (ii) preventing

exogenous species (e.g., solvent molecules) to adsorb on the surface of the Au cluster. Both of these features allow a cleaner and better-defined crystal formation, facilitating the X-ray crystal structure determination and enhancing the thermodynamic and kinetic stability of Au₁₃₃(SPh-*t*Bu)₅₂.

The UV–vis optical spectrum from time-dependent DFT simulations is reported in Figure 3a and compares reasonably well with experimental results: the features at 2.09, 2.87, and 4.1 eV are in tune with the experimental peaks at 2.49, 2.91, and [3.59–3.81] eV, with the feature at 2.09 eV red-shifted due to the use of the LDA xc-functional.¹⁹ A comparison with the spectrum of Au₁₄₄(SCH₂CH₂Ph)₆₀¹⁵ indicates a less fragmented and more pronounced optical absorption of Au₁₃₃(SPh-*t*Bu)₅₂, probably associated with increased polarizability due to the decreased thiolate density²⁰ and electron delocalization provided by phenyl conjugating. This is confirmed by a comparison with the simulated spectrum of a putative Au₁₃₃(SCH₃)₅₂ analogue (Figure S8) clearly exhibiting greater fragmentation due to quantum size effects,²¹ pointing to a non-negligible influence of conjugation on the optical response of these systems.

The ionization energy of Au₁₃₃(SPh-*t*Bu)₅₂ is modest, amounting to 4.34 eV, supporting the experimental observation of +1 as the predominant charge state (see also Figure S2). The electronic density of states of Au₁₃₃(SPh-*t*Bu)₅₂ (Figure S7) is in tune with a count of 81 free electrons and exhibits a small HOMO–LUMO gap of 0.05 eV, which increases to 0.11 eV in the Au₁₃₃(SPh-*t*Bu)₅₂⁺ cation, in excellent agreement with the lack of a band gap in voltammetry (Figure 3b). No superatom electronic shell closure and related stability are observed:^{12,22,23} the stability of Au₁₃₃(SPh-*t*Bu)₅₂ is due to the geometric factors,^{18,22} with the geometric shell closings²³ of 1 + 12 + 42 + 52 atoms (Figure 1). Indeed, the energy gain due to electronic shell closure should amount to no more than 0.5–0.6 eV at this size,^{24,25} thus being minor with respect to geometric effects.¹⁷

The achievement of such an unprecedented size is theoretically rationalized as being due to the presence of rigid and bulky –SPh-*t*Bu ligands which act as an outer protective layer, internally reducing the structural freedom of the cluster and externally preventing contamination by exogenous species. Employing bulky and rigid ligands may offer one solution to the nanostructure problem and facilitate the crystal structure determination of even larger nanomolecular materials.

■ ASSOCIATED CONTENT

📄 Supporting Information

Detailed synthetic conditions, additional mass spectra, theoretical analysis, cif file, crystal structure data and coordinates. CCDC number is 993929 (submitted Mar 27, 2014; updated Mar 8, 2015). This material is available free of charge via the Internet at <http://pubs.acs.org>.

■ AUTHOR INFORMATION

Corresponding Author

*amal@olemiss.edu

Present Address

[†]Intel Corporation, 2501 NW 229th Avenue, Hillsboro, OR 97124, USA.

Author Contributions

[#]S.T., P.R.N., L.S., and G.B. contributed equally.

Notes

The authors declare no competing financial interest.

■ ACKNOWLEDGMENTS

This work was funded through NSF-CHE-1255519. We thank Ilia A. Guzei for assistance with crystal structure solution; Nanfeng Zheng, Kevin Gagnon, Alberto Albinati, and Jared Delcamp for discussions; and the reviewers for suggestions on the structural description and refinement. Work performed at Argonne and use of the Advanced Photon Source, an Office of Science User Facility operated for the U.S. Department of Energy (DOE) Office of Science by Argonne National Laboratory, were supported by the U.S. DOE under Contract No. DE-AC02-06CH11357. Computational research was performed in part using EMSL, a DOE Office of Science User Facility sponsored by the Office of Biological and Environmental Research and located at Pacific Northwest National Laboratory.

■ REFERENCES

- (1) Whetten, R. L.; Khoury, J. T.; Alvarez, M. M.; Murthy, S.; Vezmar, I.; Wang, Z. L.; Stephens, P. W.; Cleveland, C. L.; Luedtke, W. D.; Landman, U. *Adv. Mater.* **1996**, *8*, 428.
- (2) Murray, R. W. *Chem. Rev.* **2008**, *108*, 2688.
- (3) Alvarez, M. M.; Khoury, J. T.; Schaaff, T. G.; Shafiqullin, M. N.; Vezmar, I.; Whetten, R. L. *J. Phys. Chem. B* **1997**, *101*, 3706.
- (4) Daniel, M.-C.; Astruc, D. *Chem. Rev.* **2003**, *104*, 293.
- (5) Billinge, S. J. L.; Levin, I. *Science* **2007**, *316*, 561.
- (6) Jadzinsky, P. D.; Calero, G.; Ackerson, C. J.; Bushnell, D. A.; Kornberg, R. D. *Science* **2007**, *318*, 430.
- (7) Heaven, M. W.; Dass, A.; White, P. S.; Holt, K. M.; Murray, R. W. *J. Am. Chem. Soc.* **2008**, *130*, 3754.
- (8) Qian, H.; Zhu, M.; Wu, Z.; Jin, R. *Acc. Chem. Res.* **2012**, *45*, 1470.
- (9) Mednikov, E. G.; Jewell, M. C.; Dahl, L. F. *J. Am. Chem. Soc.* **2007**, *129*, 11619.
- (10) Tran, N. T.; Powell, D. R.; Dahl, L. F. *Angew. Chem., Int. Ed.* **2000**, *39*, 4121.
- (11) Schaaff, T. G.; Shafiqullin, M. N.; Khoury, J. T.; Vezmar, I.; Whetten, R. L. *J. Phys. Chem. B* **2001**, *105*, 8785.
- (12) Lopez-Acevedo, O.; Akola, J.; Whetten, R. L.; Gronbeck, H.; Hakkinen, H. *J. Phys. Chem. C* **2009**, *113*, 5035.
- (13) See Supporting Information.
- (14) Dass, A.; Stevenson, A.; Dubay, G. R.; Tracy, J. B.; Murray, R. W. *J. Am. Chem. Soc.* **2008**, *130*, 5940.
- (15) Weissker, H. C.; Escobar, H. B.; Thanthirige, V. D.; Kwak, K.; Lee, D.; Ramakrishna, G.; Whetten, R. L.; López-Lozano, X. *Nat. Commun.* **2014**, *5*, 3785.
- (16) Quinn, B. M.; Liljeroth, P.; Ruiz, V.; Laaksonen, T.; Kontturi, K. *J. Am. Chem. Soc.* **2003**, *125*, 6644.
- (17) Reimers, J. R.; Wang, Y.; Cankurtaran, B. O.; Ford, M. J. *J. Am. Chem. Soc.* **2010**, *132*, 8378.
- (18) Crasto, D.; Barcaro, G.; Stener, M.; Sementa, L.; Fortunelli, A.; Dass, A. *J. Am. Chem. Soc.* **2014**, *136*, 14933.
- (19) Perdew, J. P.; Burke, K.; Ernzerhof, M. *Phys. Rev. Lett.* **1996**, *77*, 3865.
- (20) Sementa, L.; Marini, A.; Barcaro, G.; Negreiros, F. R.; Fortunelli, A. *ACS Photonics* **2014**, *1*, 315.
- (21) Lermé, J.; Baida, H.; Bonnet, C.; Broyer, M.; Cottancin, E.; Crut, A.; Maioli, P.; Del Fatti, N.; Vallée, F.; Pellarin, M. *J. Phys. Chem. Lett.* **2010**, *1*, 2922.
- (22) Dass, A. *Nanoscale* **2012**, *4*, 2260.
- (23) Martin, T. P. *Phys. Rep.* **1996**, *273*, 199.
- (24) Barcaro, G.; Fortunelli, A.; Rossi, G.; Nita, F.; Ferrando, R. *J. Phys. Chem. B* **2006**, *110*, 23197.
- (25) Ferrando, R.; Fortunelli, A.; Rossi, G. *Phys. Rev. B* **2005**, *72*, 085449.